HARDENABILITY OF SINTERED Fe-B-C ALLOYS

G. Saroop*, R.J. Causton ** and A. Lawley*

*Department of Materials Engineering
Drexel University, Philadelphia, PA 19104

**Hoeganaes Corporation
Cinnaminson, NJ 08077

ABSTRACT

The objective of this study was to evaluate and interpret the effect of small additions of boron (<0.09 w/o) on the hardenability of sintered Fe-B-0.3 w/o C alloys. For comparison, in terms of hardness response, binary Fe-B alloys were also evaluated. The alloys were prepared by mixing gas atomized Fe-12 w/o B with Ancorsteel 85 HP powder; carbon was added in the form of graphite. Jominy bars were fabricated from the alloy powder by cold isostatic pressing (414 MPa) in a polyurethane bag and sintering at 1120 °C or 1230 °C (30 min) in dry hydrogen (dewpoint – 40 °C). Hardenability was quantified by means of the standard Jominy end quench test. Small additions of boron enhance both the hardness and hardenability of the base Fe-C alloy, particularly at the higher sintering temperature. This effect is attributed to inhibition of the nucleation of ferrite by the boron which retards the formation of pearlite.

INTRODUCTION

Powder metallurgy (P/M) processes are growing in importance because, with this metal working technology, it is possible to fabricate high quality, complex parts to close tolerances. P/M is also economical because there is no wastage of material due to machining. Most P/M processes involve fabrication in the solid state and this avoids the segregation of alloying elements and other defects associated with conventional casting processes.

Press + sinter P/M parts contain pores, which have a detrimental effect on mechanical properties because they promote crack initiation [1]. Thus, for critical load bearing applications, it is necessary to reduce porosity by increasing the sintered density. Approaches to increasing sintered density include: increasing the compaction pressure; increasing the sintering temperature; and by utilizing liquid phase sintering.

The addition of alloying elements can enhance liquid phase sintering. For example, boron forms a eutectic (Fe-Fe_2B) with iron at 1175 ^{o}C [2,3] and above this temperature the liquid phase improves sintering. Without boron, liquid phase sintering occurs at a much higher temperatures

in the Fe-C system. Hence the addition of specific alloying elements like boron obviates the need for higher sintering temperatures.

The role of boron (up to 0.8 w/o) in enhancing the sinterability of iron has been studied by German et al. [2,3]. It was found that increasing boron additions resulted in a higher volume fraction of the liquid phase, a higher sintered density, a lower volume fraction of porosity and rounded pores. The improvement in sintered density was reflected in higher strength and hardness, while rounding of the pores resulted in enhanced ductility.

In recent studies, Causton et al. (4) and Saroop (5) have examined the effect of small additions of B (<0.09 w/o) on the sintering response of Fe-B and Fe-B-C alloys, particularly above 1175 °C. Enhanced sintering is reflected in higher mechanical property levels. In the Fe-B alloys, the microstructure consists of coarse equiaxed ferrite grains, independent of sintering temperature. The microstructure of the Fe-B-C alloys is a function of the B level and/or sintering temperature. As either entity increases, the microstructure consists of acicular ferrite and fine divorced pearlite. Sintering temperatures have been identified which optimize strength/ductility combinations in the Fe-B and Fe-B-C alloys.

Since small additions of boron have been shown to be beneficial in terms of sintering response and mechanical properties, the primary focus of the present study has been on the role of boron, at low concentration levels, on hardenability, as determined by the Jominy end quench test. The study also embraced attendant microstructures, by varying composition and sintering temperature.

In wrought steels, boron is known to be a potent alloying addition for enhancing hardenability at low concentrations (6). However, the addition of boron above a certain optimum level (ranging from 0.0005 w/o to 0.005 w/o, depending on the composition of the steel) produces no further increase in hardenability and might even produce a decrease in hardenability.

Hardenability is a fundamental property of a given steel and reflects the cooling rate necessary to achieve a martensitic structure. The presence of porosity does not change the critical cooling rate but alters the actual cooling rate achieved during quenching. Intuitively, it is predicted that the hardenability of a sintered steel will be lower than that of the corresponding wrought steel – a consequence of the pores present in the P/M steel with an associated decrease in thermal conductivity, and hence cooling rate. It must be recognized, however, that as the level of porosity increases, there is less mass to cool and this will offset the decrease in thermal conductivity.

Measured values of the thermal conductivity of sintered steels fall between the upper and lower bounds of the relation:

$$l_m(1-e) > l_s > l_m(1-2e) \qquad (1)$$

with a tendency to concentrate toward the lower bound. In equation (1) λ_s is the thermal conductivity of the sintered alloy, λ_m is the thermal conductivity in the absence of porosity, and ε is the fractional porosity.

The hardenability of the sintered steels depends on cooling rate. The heat that has to be removed during quenching is given by (1):

$$Q = G(1-e)C_m\Delta T \qquad (2)$$

Where G(1-ε) is the mass of sintered steel that has the same surface for heat exchange as a fully dense part of the same shape and volume, C_m is the heat capacity of the fully dense steel. Q/GΔT) can be considered as the 'heat' required to increase the temperature of unit volume by 1°C, i.e. an indicator of the 'resistance' to cooling.

The cooling rate possible in a material characterized by porosity ε is given by the ratio of equation (2) and the lower bound condition in equation (1). For medium or low porosity, the cooling rate is a function of:

$$l_m(1-e)/C_m$$

Thus wrought steels (fully dense) will cool faster than porous steels, and the cooling rate will decrease with increasing porosity.

EXPERIMENTAL PROCEDURES

Materials and Alloying

The base iron powder used in this study was water atomized Hoeganaes Ancorsteel 85 HP, of composition Fe-0.85 w/o Mo-0.14 w/o Mn(C<0.01 w/o), with d_m=95 μm. The source of boron was gas atomized Fe-12 w/o B with d_m=18 μm, produced by Ultrafine Powders Technology, Inc. Characteristic of water and gas atomization, the powders were irregular in shape and spherical, respectively.

The base iron powder was mixed with the required weights of Fe-B powder and graphite (Asbury 3203 HSC; 90 w/o <10 μm) in a V cone blender for 30 min. Nominal compositions of the seven alloy mixes, evaluated in terms of carbon and boron levels, are given in Table I.

Table I: Nominal Composition of Powder Mixes (w/o).

Alloy	Composition
1	0.3C
2	0.3C + 0.03B
3	0.3C + 0.06B
4	0.3C + 0.09B
5	0.03B
6	0.06B
7	0.09B

Jominy End Quench Testing

Powders were cold isostatically compacted at 60x 10^3 psi (414 MPa) in a polyurethane bag into Jominy bars 10.16 cm (4 inches) long and 2.54 cm (1 inch) dia; no lubricant was added. Compacts from each alloying mode were sintered at two temperatures: 1120 ^{o}C and 1230 ^{o}C in a pure hydrogen atmosphere with a dew point of less than –40 °C. The compacts were placed on an alumina boat and inserted into the furnace. A steel washer 3.81 cm (1.5 inches) dia. was riveted to the top of each cylindrical specimen after machining of the cylindrical surface. The density of the bars was evaluated in the green and sintered condition gravimetrically after dimensioning.

The Jominy end quench test was carried out in accordance with ASTM A 255-96 (7). Each sample was austenitized for 30 min (940 ^{o}C for samples without carbon and 840 ^{o}C for samples containing 0.3 w/o carbon). Austenitizing was done in air in a box furnace. To prevent decarburization the bars were coated with graphite and placed in a hole in a graphite block. After austenitizing, the sample was quenched rapidly in a standard Jominy end quench fixture. The sample was kept in the fixture for at least 10 min.

Two parallel flats were ground longitudinally on the samples to a depth of at least 1mm to remove any decarburization and surface porosity. The grinding was done with water cooling. Hardness reading were taken on the Rockwell A scale for samples containing carbon, and the B scale for samples without carbon, at intervals of 1.5875 mm (0.0625 inch) beginning at the quenched end. Readings were taken for a distance of at least 5.08 cm (2 inches) from the water quenched end. Hardness was plotted as a function of distance.

Metallography

Two sections were cut perpendicular to the longitudinal axis of the Jominy bar from each of the samples. One section was located 0.318 cm (0.125 inch) from the quenched end and the other 0.318 cm (0.125 inch) from the air-cooled end. These sections were mounted in bakelite and prepared for optical microscopy using standard procedures. Optical micrographs were obtained after etching in nital.

Microindentation hardness readings were taken across the diameter of the Jominy bar to determine the extent of decarburization. The hardness (VHN) was plotted as a function of distance from the surface. On the basis of the microindentation hardness profile, the samples were ground to a depth of 1 mm.

Chemical Analyses

Carbon, sulfur, oxygen and nitrogen levels in the sintered alloys were determined using a LECO analyzer. Boron analyses were performed by means of induction coupled plasma spectrometry (ICPS).

RESULTS AND OBSERVATIONS

Sintered Alloy Compositions:

Results of the chemical analyses are shown in Table II.

Table II: Chemical Composition of Sintered Alloys.

Premix	Sintering Temperature (^oC)	Carbon (w/o)	Sulphur (w/o)	Oxygen (w/o)	Nitrogen (w/o)	Boron (w/o)
1	1120	0.21	0.004	0.032	<0.001	0.01
2	1120	0.21	0.003	0.044	<0.001	0.034
3	1120	0.27	0.003	0.048	<0.001	0.026
4	1120	0.28	0.003	0.051	0.007	0.066
5	1120	0.081	0.002	0.045	<0.001	0.020
6	1120	0.085	0.002	0.059	0.005	0.034
7	1120	0.11	0.004	0.051	0.006	0.082
1	1230	0.18	0.002	0.0092	0.0005	0.008
2	1230	0.19	0.002	0.0189	0.0005	0.017
3	1230	0.23	0.001	0.0267	0.0002	0.047
4	1230	0.23	0.001	0.0224	0.0001	0.076
5	1230	0.012	0.001	0.0177	0.0001	0.01
6	1230	0.007	<0.001	0.03	0.001	0.021
7	1230	0.005	<0.001	0.02	<0.001	0.044

At a sintering temperature of 1120 ^oC the boron levels in the Fe-B premixes 5, 6 and 7 were found to be 0.2 w/o, 0.034 w/o and 0.08 w/o B respectively. These compare with the nominal boron levels of 0.03 w/o, 0.06 w/o and 0.09 w/o.

At the same sintering temperature (1120 ^oC) the boron levels in the Fe-C-B premixes 2, 3, and 4 were found to be 0.034 w/o, 0.026 w/o and 0.066 w/o B respectively. These compare with the nominal boron levels of 0.03 w/o, 0.06 w/o and 0.09 w/o. At a given sintering temperature the boron losses in the Fe-B-C alloys (premixes 2-4) were higher than those in the Fe-B alloys (premixes 5-7). The carbon levels in these alloys were 0.21 w/o, 0.27 w/o and 0.28 w/o respectively, compared to the nominal level of 0.3 w/o C.

At a sintering temperature of 1230 ^oC the boron levels in the Fe-B premixes (5, 6 and 7) were 0.01 w/o, 0.021 w/o and 0.044 w/o respectively. These compare with the nominal boron levels of 0.03 w/o, 0.06 w/o and 0.09 w/o B respectively.

At the same sintering temperature, the B levels in the Fe-B-C premixes (2, 3 and 4) were 0.017 w/o, 0.047 w/o, and 0.076 w/o B respectively. These compare with the nominal B levels of 0.03 w/o, 0.06 w/o and 0.09 w/o B. Boron loss due to sintering in the Fe-B alloys was higher at this sintering temperature compared to alloys sintered at 1120 ^oC. Boron losses were higher in the Fe-B alloys sintered at 1230 ^oC than the boron losses in the Fe-B-C alloys sintered at the same temperature. The carbon levels in these alloys were 0.19 w/o, 0.23 w/o and 0.23 w/o C, respectively. These losses were higher at a sintering temperature of 1230 ^oC compared to alloys sintered at 1120 ^oC.

Hardenability

Green Density and Sintered Density

Green density of all the compacts were in the range 6.8-7.0 g/cm^3. Sintered density was in the range 6.9-7.1 g/cm^3.

Hardenability Curves

The ASTM standard for hardenability of wrought steels (ASTM A 255-96) requires that samples be ground to a depth of 0.5 mm. Microindentation hardness vs distance plots reveal that decarburization occurred to a depth of about 1 mm; for all the alloys, the microhardness at the surface is about 100VHN less than the microhardness at a depth of 1mm. Hence flats were ground to a depth of 1mm to avoid the effect of decarburization.

Jominy hardness profiles of the Fe-B-C alloys sintered at 1120 ^{o}C are shown in Figure 1(a). The hardness of the alloys increases with increasing boron content. The hardness at both the air-cooled end and the water quenched end increases with increasing boron content. Similar trends are observed in the Fe-B-C alloys sintered at 1230 ^{o}C as shown in Figure 1(b). The hardness of the alloys sintered at 1230 ^{o}C is higher than that of the alloys sintered at 1120 ^{o}C. The hardness curves shift upwards with increasing sintering temperature and boron content.

The Jominy hardness profiles of the Fe-B alloys sintered at 1120 ^{o}C are shown in Figure 2(a). The curves shift upwards with increasing boron content. The shift is much more pronounced compared to the Fe-B-C alloys. The shift becomes a stronger function of boron content at the higher sintering temperature of 1230^{o}C, as seen in Figure 2(b).

The Jominy hardness profile for a wrought AISI - 1018 steel is shown in Figure 3. The carbon level in this steel is lower than the levels in the Fe-B-C steels examined in this study. However, the AISI - 1018 steel contains Mn (0.6-0.9 w/o) which enhances hardenability significantly. The hardness of the wrought steel is higher than that of the P/M steels because of porosity in the latter. The rate of decrease in hardness with distance from the water quenched end of the Jominy bar is higher in the wrought steel than in the porous Fe-B-C P/M steels.

Microstructures

Representative microstructures from the water quenched end of the Jominy bars of alloys Fe-0.3 w/o C, Fe-0.3 w/o C – 0.03 w/o B and Fe-0.3 w/o C – 0.09 w/o B sintered at 1120 °C are compared in Figures 4(a), 4(b) and 4(c). Martensite is present in each alloy (acicular/needle-like morphology) but is coarser in the alloy with the highest boron content.

At the air-cooled end of the Jominy bars of the three alloys sintered at 1120 °C, pearlite and ferrite are present. The morphology of the pearlite is more acicular in the alloy with the highest boron content, similar to the as-sintered microstructures.

Representative microstructures from the water quenched end of the Jominy bars of alloys Fe-0.3 w/o C, Fe-0.3 w/o C–0.03 w/o B and Fe-0.3 w/o C-0.09 w/o B sintered at 1230 °C are compared

in Figures 5(a), 5(b) and 5(c). In the boron-free alloy, very fine needles of martensite are present. Compared to the lower sintering temperature, there are fewer and more-rounded larger pores. In the two alloys containing boron, martensite is present but is coarser than that present after sintering at 1120 °C. In addition, white areas are visible which are probably regions of ferrite or carbides containing boron.

At the air-cooled end of the Jominy bars of the three alloys sintered at 1230 °C, pearlite and ferrite are present. In the boron-free alloy the pearlite is finer than that present after sintering at 1120 °C. The pearlite assumes a more acicular morphology with increasing boron content, similar to the as-sintered microstructures.

Representative microstructures of the water quenched end of the Jominy bars of the Fe-0.03 w/o B and Fe-0.09 w/o B alloys sintered at 1120 °C are compared in Figures 6(a) and 6(b). Equiaxed grains of ferrite and pores are seen in the alloy of lower boron content. In contrast, the ferrite is acicular in the Fe-0.09 w/o B alloy.

At the air-cooled end of the Jominy bars of the Fe-0.03 w/o B alloy sintered at 1120 °C, the ferrite grains are equiaxed. In the alloy of higher boron content, the ferrite is acicular. Pores are evident in each microstructure.

Representative microstructures at the water quenched end of the Jominy bars of the Fe-0.03 w/o B and Fe-0.09 w/o B alloys sintered at 1230 °C are compared in Figures 7(a) and 7(b). Equiaxed grains of ferrite and pores are present in the alloy of lower boron content. In contrast the ferrite exhibits an acicular morphology in the Fe-0.09 w/o B alloy. In both alloys the pores are larger and more rounded than those in the alloys sintered at 1120 °C.

At the air-cooled end of the Jominy bar of the Fe-0.03 w/o B alloy sintered at 1230 °C, the ferrite grains are equiaxed. In the alloy of higher boron content, the ferrite is acicular. Compared to the lower sintering temperature, the pores are larger and more rounded.

DISCUSSION

Composition of Sintered Alloys

The nominal and sintered compositions of the Fe-B alloys are given in Tables I and II respectively. The data shows that each alloy loses boron during sintering. This is attributed to the formation of B_2O_3 which vaporizes at the sintering temperature. The magnitude of the boron loss increases with increasing sintering temperature. The remaining boron is in solid solution and possibly in the form of Fe_2B since the Fe-Fe_2B eutectic forms at a temperature of 1175 ^oC (8).

As seen in Tables I and II there is some carbon loss in each of the Fe-B-C alloys. This could be due to the reaction of carbon with hydrogen to form CH_4 gas. Since the dew point of the sintering atmosphere was less than –40 ^oC, it is unlikely that CO and/or CO_2 will form. Most of the Fe-B-C alloys lose boron during sintering, similar to the behavior of the Fe-B alloys. The remaining boron is in solid solution and possibly in the form of $Fe_3(C,B)$ based on the ternary phase diagram (9)

The oxygen concentration is very low in each of the alloys (Tables I and II). This is attributed to the low dew point (-40 ^{o}C) of the sintering atmosphere. The low nitrogen content of the alloys is the result of the dynamic flow of hydrogen during sintering.

Distribution of Alloying Elements

Chemical inhomogeneity can arise from segregation when powders of different sizes, shapes, and densities are mixed together. The Fe-B ferroalloy powder is much finer (d_m=18 μm) than the Ancorsteel 85 HP iron base powder (d_m=95 μm). The density of the Fe-B master alloy is 5g/cm^3 whereas the density of Ancorsteel 85 HP is close to 7.9 g/cm^3. The water atomized
Ancorsteel 85 HP powder is irregular in shape whereas the gas atomized Fe-B alloy is spherical. Thus, some degree of chemical inhomogeneity is expected. Confirmation of chemical inhomogeneity is difficult because the detection of boron below 1w/o is not possible using EDX, WDX or Auger spectroscopy (10). SIMS (11) can be employed to characterize quantitatively the distribution of boron in the alloys.

Hardenability

Boron is added to steels to enhance hardenability. To be effective boron has to be in solid solution. The hardenability curves of P/M steels are different from those of wrought steels in two ways. Since P/M steels are softer (because of porosity) the hardness scales used are generally HRB or HRF compared to HRC in the case of wrought steels. As confirmed in the introduction, P/M steels have a lower thermal conductivity than their wrought counterparts. Thus, the cooling rate during the quenching of a P/M part will be lower than that in the wrought metal part.

With an increase in sintered density, thermal conductivity increases. This means that, at a given distance from the water cooled end of the Jominy bar, the cooling rate increase with increase in the sintered density. As a result, hardness is retained to a greater depth and hardenability is increased. This is seen by comparing Figures 1 (a) and 1(b)

Boron enhanced the hardness of both the Fe-B-C alloys and the Fe-B alloys. In the Fe-B-C alloys the microstructure at the quenched end changed significantly with additions of boron. As the boron level increased the martensite needles became coarser and there was less retained austenite. In the Fe-B alloys the morphology of the ferrite changed from equiaxed to acicular. This is because boron segregates to grain boundaries and prevents heterogeneous nucleation of ferrite (12).

Boron is an α stabilizer and carbide former (13). Carbide formers reduce the rate of growth of pearlite and proeutectoid ferrite by a solute drag effect on the moving γ / α interface (14). It has also been suggested that B poisons ferritic nucleation sites by the precipitation of carbide clusters in grain boundaries (12,14). Again this slows down the $\gamma \Rightarrow \alpha + Fe_3C$ reaction and promotes the transformation of γ into martensite, thus enhancing the hardenability of the steel.

Another mechanism by which boron enhances the hardenability of steels is by the formation of the fcc borocarbide $Fe_{23}(C,B)_6$ at austenite grain boundaries (15). The borocarbide forms a coherent boundary with one austenite grain and a noncoherent boundary with the other. The

coherent boundary is not a suitable site for ferrite nucleation. This inhibits ferrite nucleation and hence slows down the $\gamma \Rightarrow \alpha + P$ reaction, thereby improving hardenability.

CONCLUSIONS

- Jominy bars can be fabricated from the premixed powders by cold isostatic pressing.
- Small levels of boron (<0.07 w/o) can be retained in the sintered Fe-B and Fe-B-C alloys
- The boron exerts a strong influence on the sintering response of the alloys, particularly above 1175 °C.
- Hardness and hardenability of the sintered Fe-B-c alloys, determined via the Jominy end-quench test, are increased by these small additions of boron.

ACKNOWLEDGMENT

Gautam Saroop is indebted to the Hoeganaes Corporation for financial support as a graduate student at Drexel University.

REFERENCES

1. G.F. Bochini, “The Influence of Porosity on the Characteristics of Sintered Materials”, The International Journal of Powder Metallurgy, 1986, Vol. 22, No.3, p.185
2. D.S. Madan and R.M. German, “Structure Property Relationship in Iron Powder Compacts Alloyed with Boron”, Advances in Powder Metallurgy, compiled by T.G. Gasbarre and W.F. Jandeska, Metal Powder Industries Federation, Princeton, N.J., 1989, Vol. 1, p.147
3. H. Zhang, R.M. German, R.T. Fox and D. Lee “Enhanced Sintering of Injection Molded Iron Alloyed with Mo, B, Ni and P”, Advances in Powder Metallurgy, compiled by E.R. Andreotti and P.J. McGeehan, Metal Powder Industries Federation, Princeton, N.J., 1990, Vol. 1, p.483
4. R.J. Causton, J-S. Oh, and A. Lawley, “Processing, Microstructure and Mechanical Properties of Fe-B and Fe-B-C Alloys”, Advances in Powder Metallurgy and Particualte Materials – 1999, Compiled by C.L. Rose and M.H. Thibodeau, Metal Powder Industries Federation, Princeton, NJ, Vol. 2, Part 7, p. 3, 1999.
5. G. Saroop, “Microstructure, Mechanical Properties and Hardenability of Sintered Fe-B and Fe-B-C Alloys”, 2000, M.S. Thesis, Drexel University, Philadelphia, PA.
6. H.E. McGannon, “The Making and Shaping of Iron and Steels”, United States Steel Corporation, Ninth Edition, 1971, p.1133
7. “Standard Test Method for End-Quench Test for Hardenability of Steel”, 1996, ASTM, A 255-96
8. O. Kubaschewski, Iron Binary Phase diagrams, 1982, Springer-Verlag, Dusseldorf, Germany, p.15
9. L. Borlera and M.G. Pradelli, “Solid State Equilibria in the Fe-B-C Systems”, La Metallurgia Italiana, 1967, Vol. 11, p.907
10. A.M. Ilyin and V.N. Golovanov, “Auger Spectroscopy Study of the Stress Enhanced Impurity Segregation in a Cr-Mo-V Steel”, Journal of Nuclear Materials, 1996, Vol. 233-237, p.233

11. W.H. Gourdin, S.L. Weinland and G.H. Campbell, “Mechanical Behavior of Diffusion-Bonded Bicrystals of Boron-Doped Ni_3Al”, Materials Science and Engineering, 1997, Vol A222, p.28.
12. R. Honeycombe, H.K.D.H. Bhadeshia, “Steels, Microstructures and Properties”, 1996, Arnold, London
13. L. Labrecque and M.Gagne, “Ductile Iron: Fifty Years of Continuous Development”, Canadian Metallurgical Quarterly, 1998, Vol 37, No. 5, p.343.
14. D.A. Porter and K.E. Easterling, “Phase Transformations in Metals and Alloys”, second edition, 1992, Chapman and Hall, New York, NY, p.343
15. W.C. Leslie, “The Physical Metallurgy of Steels”, 1981, Hemisphere Publishing Corporation, New York, p.276.

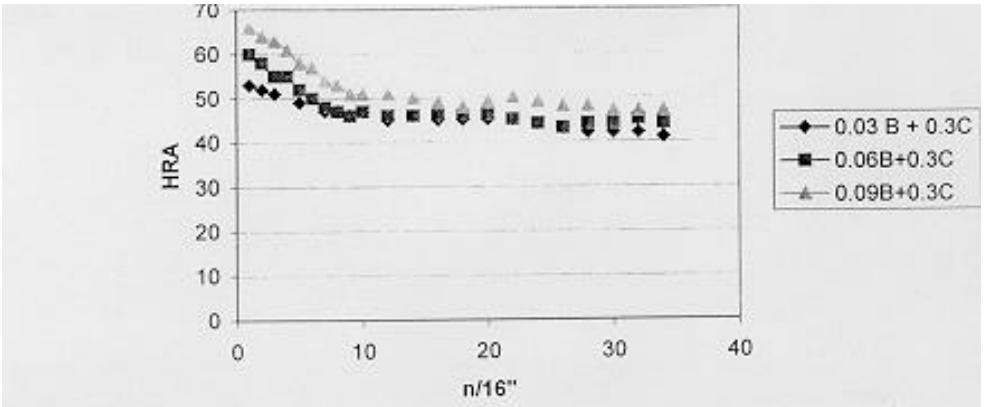

Figure 1(a): Jominy hardness traces for Fe-B-C alloys sintered at 1120 °C.

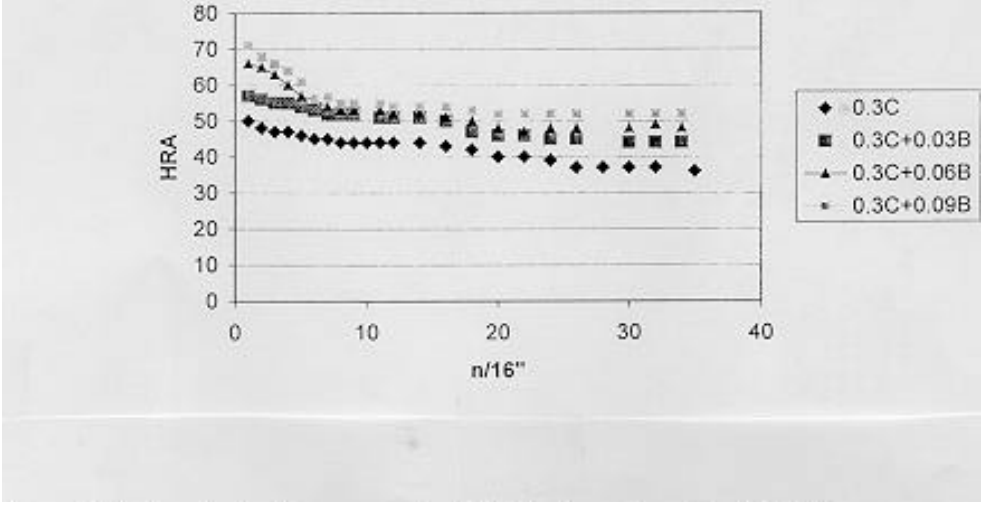

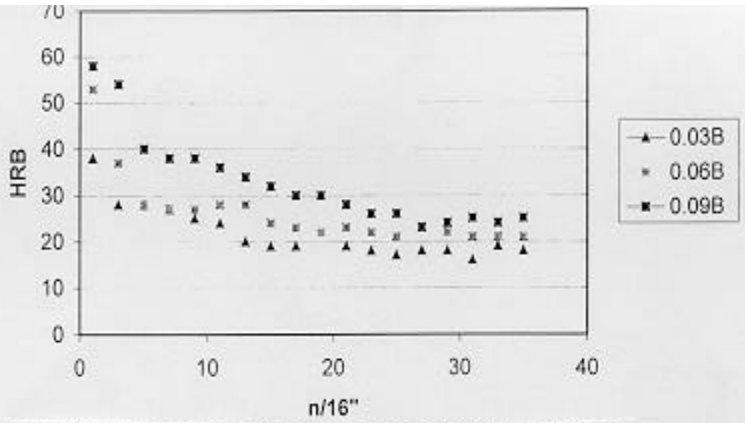

Figure 2(a): Jominy hardness traces for Fe-B alloys sintered at 1120 °C.

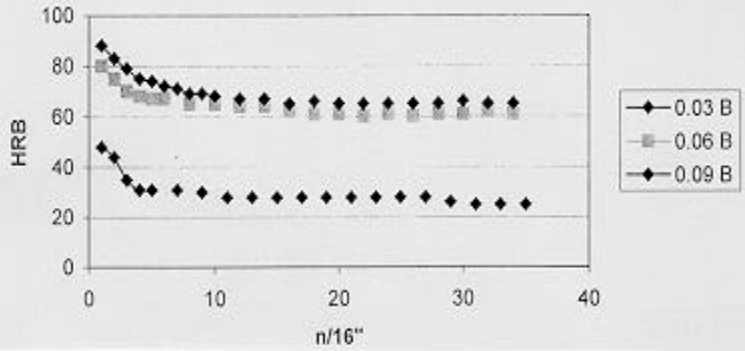

Figure 2(b): Jominy hardness traces for Fe-B alloys sintered at 1230 °C.

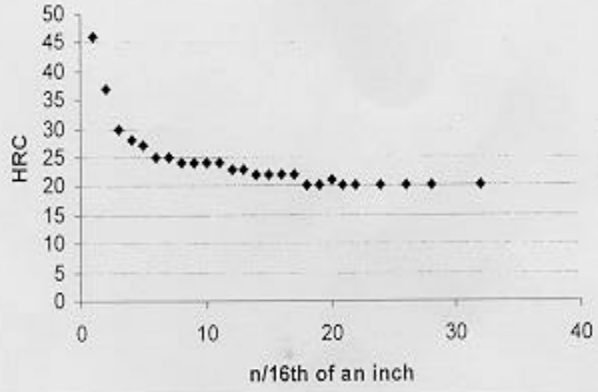

Figure 3: Jominy hardness trace for wrought AISI - 1018 steel.

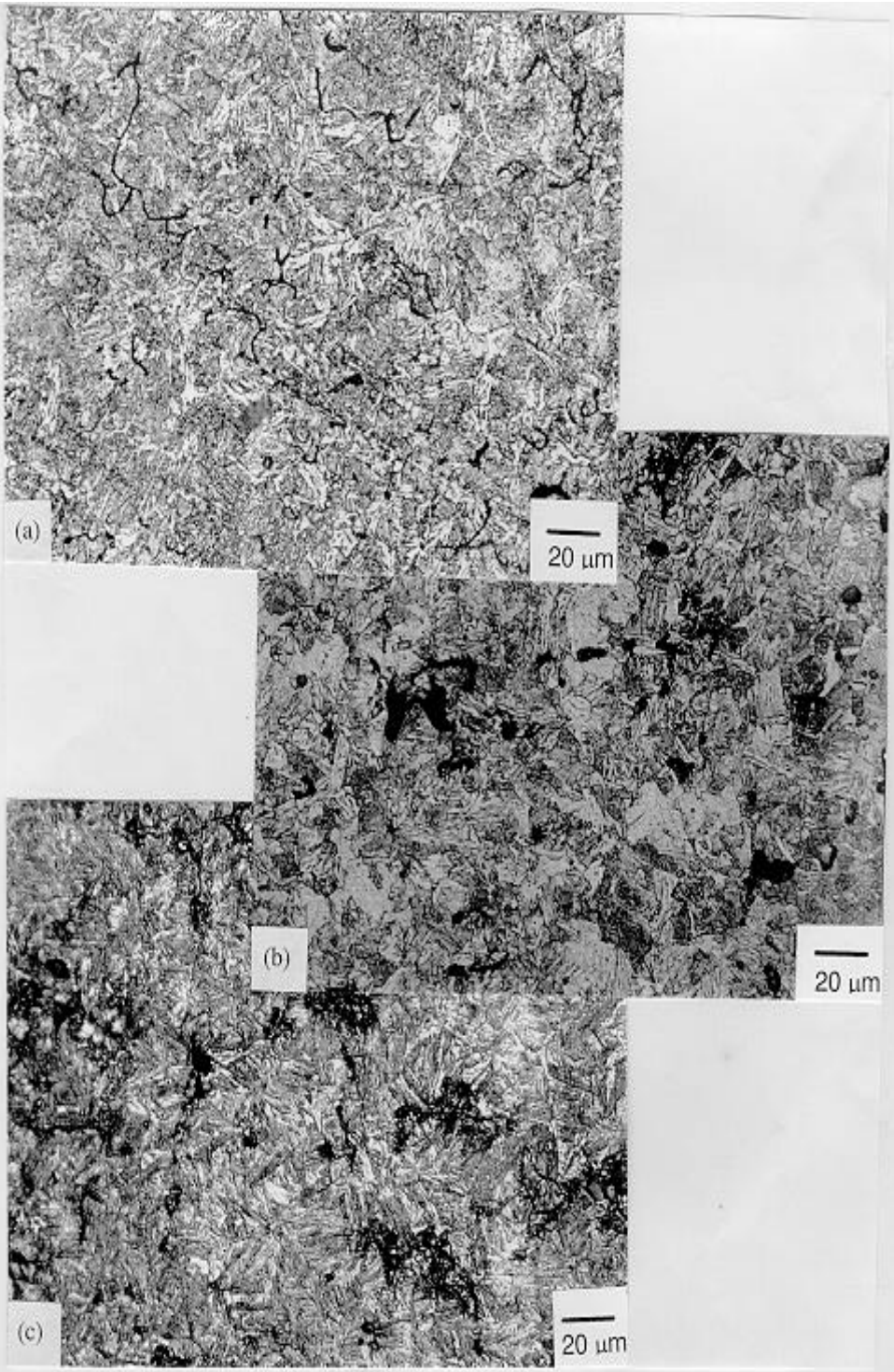

Figure 4: Microstructures at water quenched end of Jominy bars: (a) Fe-0.3 w/o C, (b) Fe-0.3 w/o C – 0.03 w/o B, (c) Fe-0.3 w/o C – 0.09 w/o B. Alloys sintered at 1120 °C; optical micrographs.

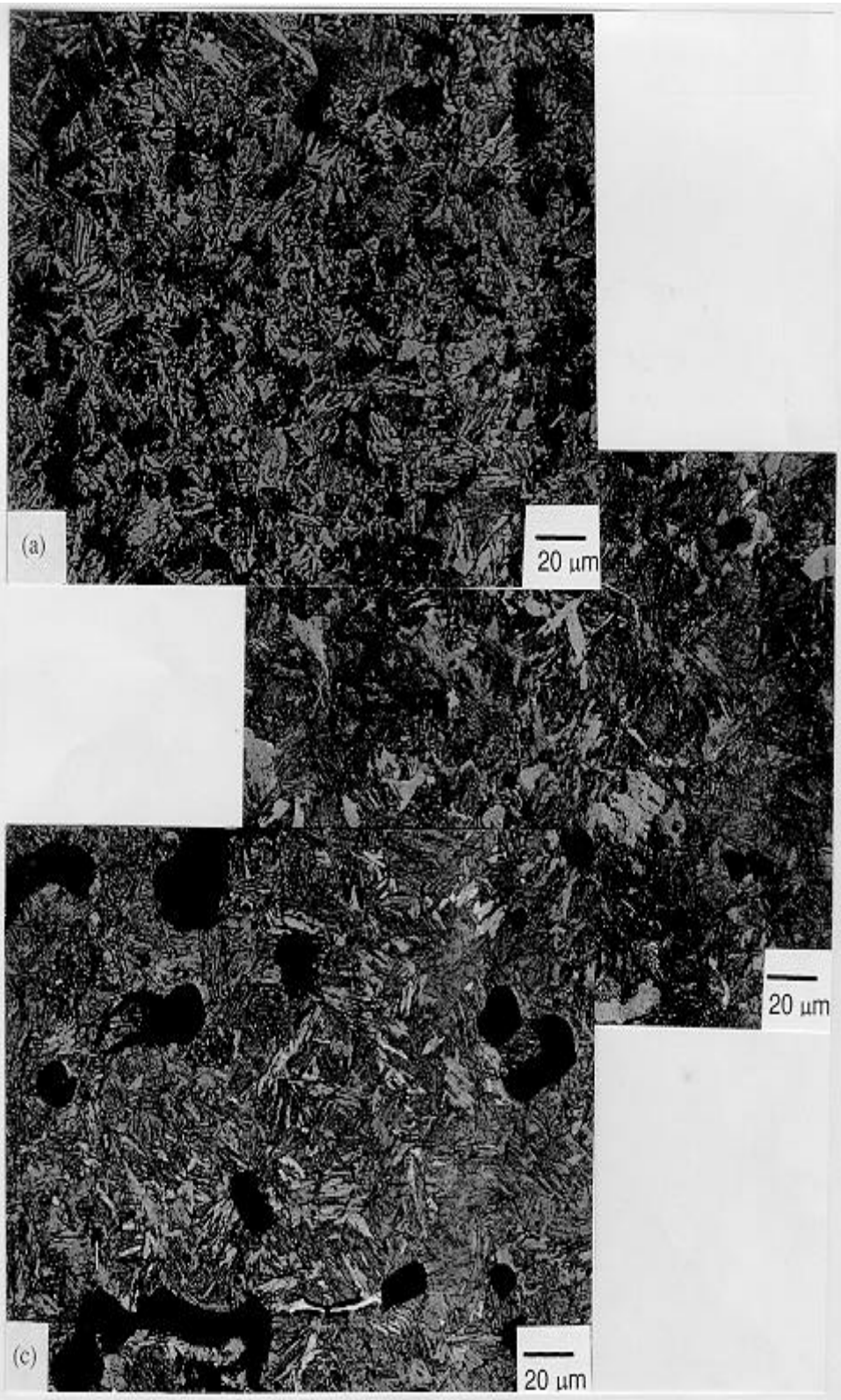

Figure 5: Microstructures at water quenched end of Jominy bars: (a) Fe-0.3 w/o C, (b) Fe-0.3 w/o C – 0.03 w/o B, (c) Fe-0.3 w/o C – 0.09 w/o B. Alloys sintered at 1230 °C; optical micrographs.

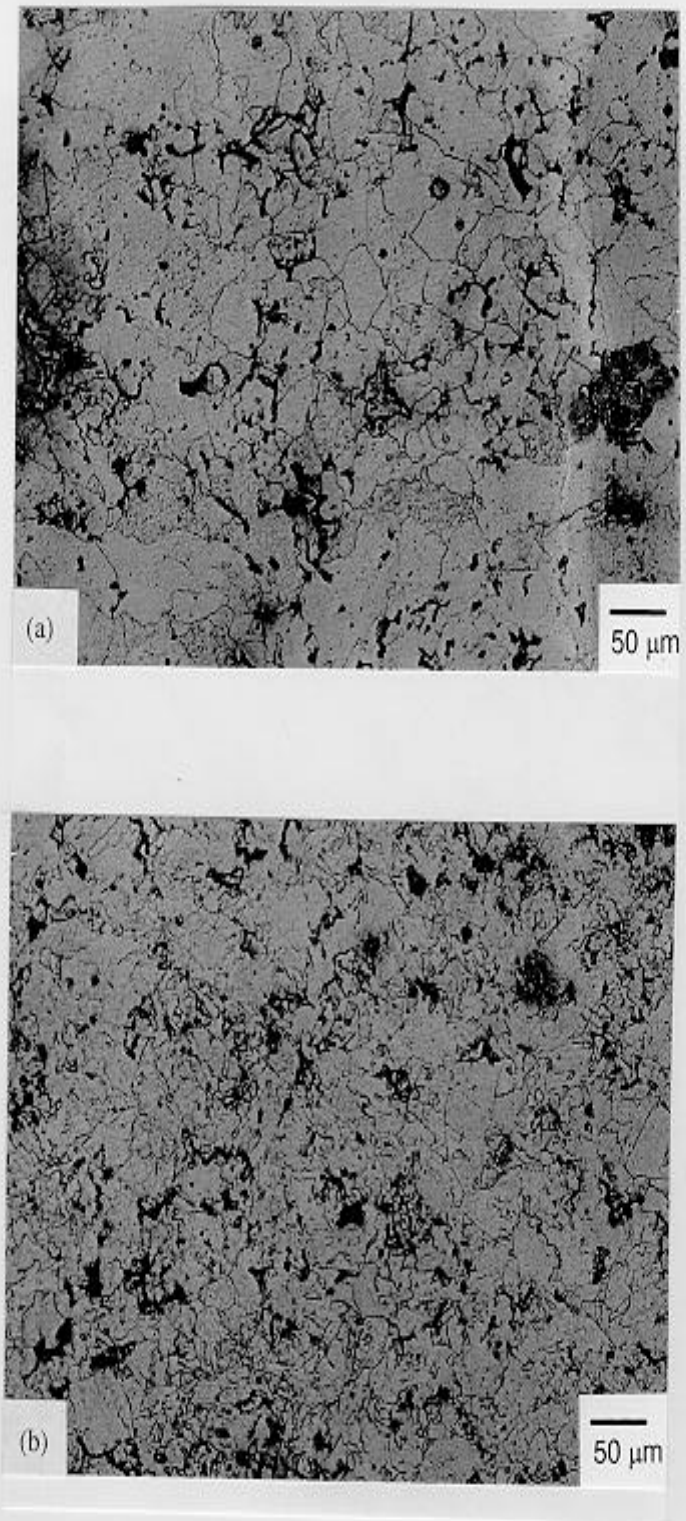

Figure 6: Microstructures at water quenched end of Jominy bars: (a) Fe-0.03 w/o B, (b) Fe – 0.09 w/o B. Alloys sintered at 1120 °C; optical micrographs.

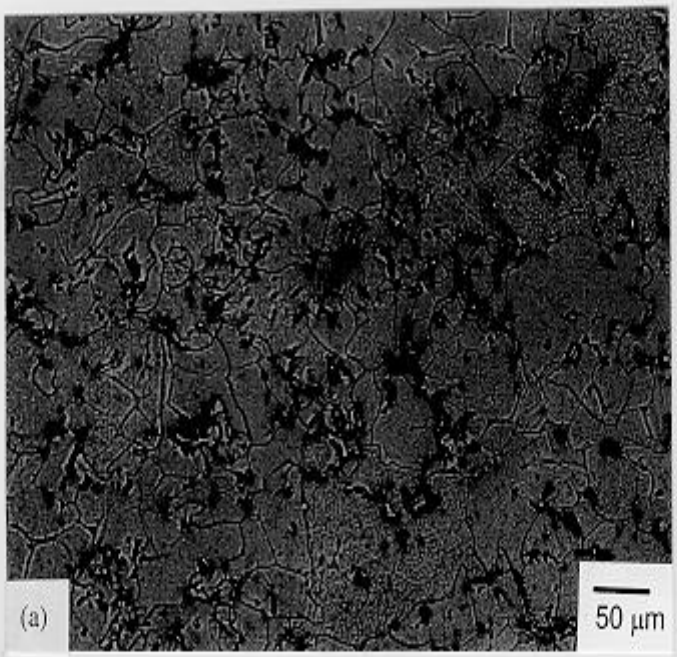

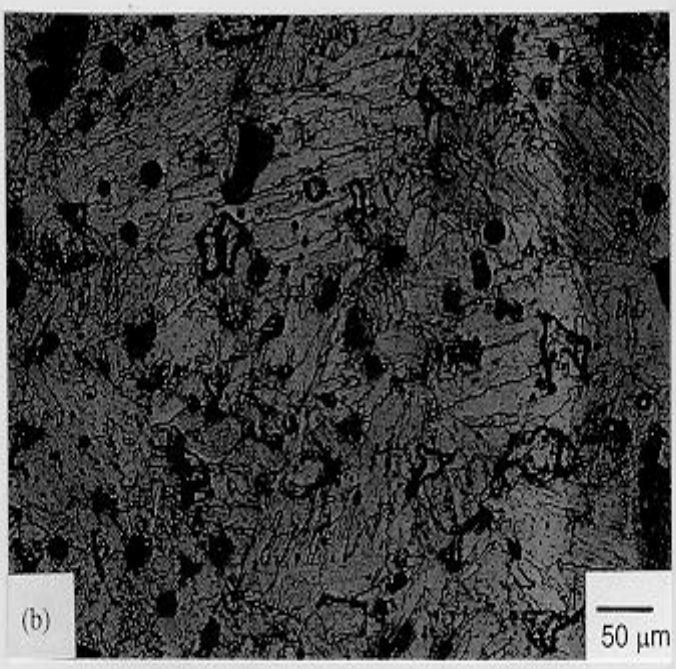

Figure 7: Microstructures at water quenched end of Jominy bars: (a) Fe-0.03 w/o B, (b) Fe – 0.09 w/o B. Alloys sintered at 1230 °C; optical micrographs.